Analysis of the O-rings that influence the performance of RCP hydrostatic seal based on TEH coupling method

Jianghong Zhang [1], Kan Chen [2], Yijin Ma [1], Mingzhong Feng [2], Wei Liu [2], Junkai Zhang [2], Hebin Ren [2]

[1] Suzhou Nuclear Power Research Institute, China General Nuclear Power Corporation, Shenzhen 518026, China
[2] Department of Nuclear Equipment, Sichuan Sunny seal company Co., Ltd, Chengdu 610031, China

Abstract: A Multi-body contacting Thermal-Elastic-Hydro Model, MTEHM has been established in this study. And which has been applied to analysis the leakage behavior of No.1 seal of the RCP hydrostatic seal. The hydro-model is based on 2D Reynolds equation and programmed by M-code. An interface program written in C has been carried out. And which is used to transit the end face pressure value from hydro-model to elastic-solid model. The FEA multi-body contacting method has been taken into the elastic-solid model. And which is used to obtain the deformation angle of seal rings. An opening force ratio has been carried out as a convergent judgment of the multi-physics iterative coupling process. The influence of position of O-rings (on the back of seal rings and relative to the hydrostatic clamp rings) has been discussed. For test and verify the MTEHM, a testing rig has been established. It can be used to simulate a high temperature high pressure seal media with a temperature range from 22℃ to 100℃ and a pressure range from 0.1MPa to 22MPa. At last, a comparison of pressure-leakage data from Westinghouse, Saint Alban power plant and this study has been presented. And a variance analysis has been attached.

Key words: hydrostatic seal; RCP; RCP seal; multi-physics coupling; TFSI.

1. Introduction

Reactor coolant pump (RCP) is used to transport media for cooling down the reactor core and exchanging heat. The hazardous high pressure media is separated by RCP seal from ambient. The performance of this seal influence safety and stability of whole nuclear power plant directly. A hydrostatic RCP seal which is applied on Chinese generation-III PWR is shown as Fig. 1. It contains three mechanical seals which are arranged tandem. The No.1 seal has two silicon nitride seal rings. One of which is rotating relative to another. The stationary ring has a taper with several minutes. The pressure difference between inner and outer of the end face make the seal rings separated from each other with a 10um gap. Usually, the differential pressure is 15.5MPa and with a 700L/h leakage. The No.1 seal subject to the whole working pressure so it is the most significant sub-part in the whole RCP seal[1-2]. In normal work condition, the No.2 seal subjected to 0.02~0.2MPa differential pressure and has an 18L/h leakage. In emergence work condition, the type of No.2 Seal will be changed from rub seal to non-contacting seal and keep the seal function for at least another 30 minutes[2].

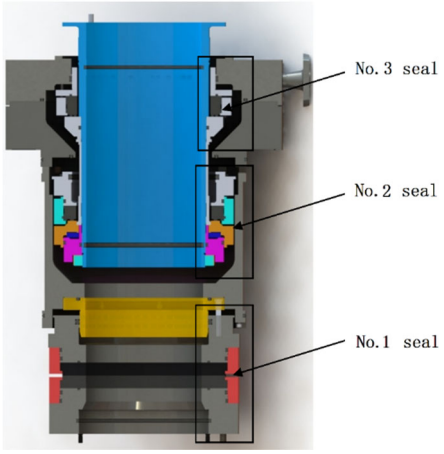

Fig. 1. Hydrostatic RCP seal assemble

The No.3 seal has a dual-dam. The block media is supplied by a high tank and injected into the end face by several orifices. No.3 seal has a leakage of hundreds milliliter per hour which is too small to be measured by general flow meter but it can be measured by weighing[2]. Considered the importance of No.1 seal, an enhanced research is necessary.

A large number of institutes and researchers have published their theoretical and experimental study results. T. Boardman from Rockwell has established a hydrostatic calculation model for dual-taper RCP seal based on Bernoulli's equation[3]. An inlet pressure loss factor has been introduced. But the structure deformation caused by pressure and temperature has not been taken into his model. The pressure-leakage curve carried out by this model is linear. Which is not suit to the real situation from power plants (in fact it is similar to convex curve)[4]. Noël Brunetiere etc. have taken the inertia term into their model [5], but it is pure fluid model also. Wang Heshun has established a brief explicit model but solid deformation is still not being considered[6]. Yasuhiro Sasaki etc. have analyzed No.1 seal rings' deformation and optimized the design by increase axial dimension to increase operational stability[7]. Liao Chuanjun etc. from Tsinghua University have considered the end face deformation caused by pressure[8]. They have deduced this deformation angle by stress analysis of ring's section. And then the gap function with end face deformation has been carried out. A solid-fluid coupled model has been established at last. But in their research, only a single ring's section has been analyzed. The interaction between rings, clamp rings and ring seats has been ignored. Especially, the clamping force induced by differential pressure on the clamp rings has been ignored. WeiFeng Huang etc. from Tsinghua University also has presented their TFS model to analysis RCP No.1 seal. The interaction of rotating parts has been considered, but the clamping force produced by clamp ring's two O-rings with different diameters has been ignored in their research[9].
Therefore, to establish a multi-body contacting thermal-Elastic-hydro-coupling model and use it to analysis No.1 seal leakage behavior is significant.

2. Structures and Function of No.1 Seal

As shown in Fig. 2, the sealing boundary consists with rotating component, stationary component and insert. Rotating ring, hydrostatic clamp ring and rotating ring seat are assembled as the rotating component. Stationary ring, hydrostatic clamp ring and stationary ring seat are assembled as the stationary component. Seal rings are made of Si3N4. The stationary ring has a taper approximate equal to 2.8 minutes.

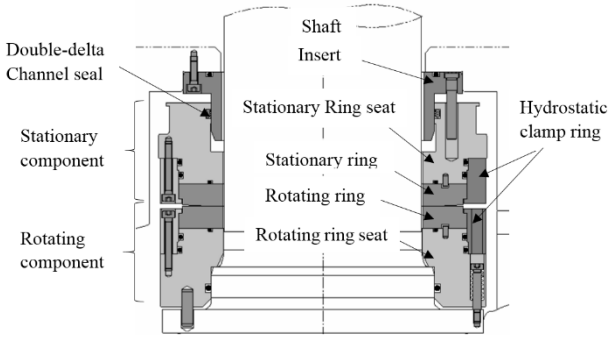

Fig. 2. No.1 seal assemble

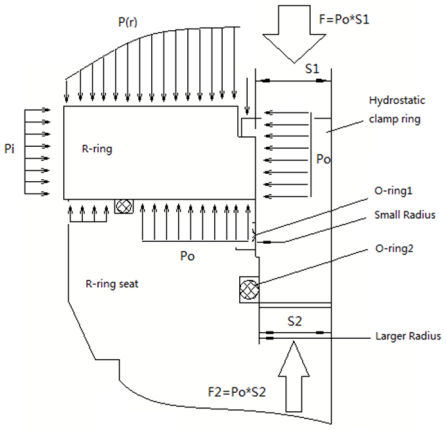

Fig. 3. Ring section and subject to force

What needs to be emphasized is that the seal rings are not bond with seats by screws and clamp rings mainly. The initial load of these screws is very small about 1.5Nm. In fact, an axial hydrostatic force ($F - F_2$, as shown in Fig. 3) produced by two O-ring with different radius push the rings onto seats tightly. So that the clamp rings are named "hydrostatic clamp rings" strictly. The hydro-load has a range from 0 to 14809.2N when media pressure is between 0~15.5MPa.

3. Hydrostatic Model of the End Face

As shown in Fig. 4. It is assumed that the ring section rotate φ_r, φ_s relative to initial position when subjected to pressure and thermal gradient. Then the end face film thickness will be changed. End face pressure distribution changed as well as. The end face opening force and leakage will be changed at last.
Nomenclature

R_o — Outer radius of rotating ring, mm

R_i — Inner radius of rotating ring, mm

R_g —End face taper transition radius, mm

R —Radial variable, mm

φ_r —Deflection angle of rotating ring, minutes

φ_s —Deflection angle of stationary ring, minutes

$\Delta\varphi$ —total deflection angle of end face, minutes, $\Delta\varphi = \varphi_s + \varphi_r$

φ_t —initial taper of end face, minutes

$\varphi_t^{'}$ —net angle of end face after deformation, minutes, $\varphi_t^{'} = \varphi_t - \Delta\varphi$

h_a —film thickness of end face parallel region, μm

h_b —film thickness of end face taper region, μm
G—gravity of stationary component, N
F_{open} —end face open force, N
F_{close} —end face close force, N

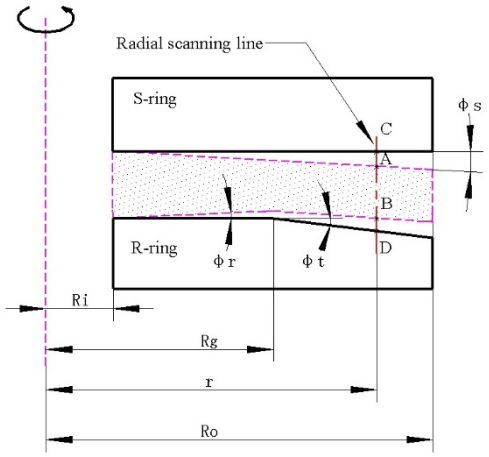

Fig. 4. No.1 seal end face dimensions

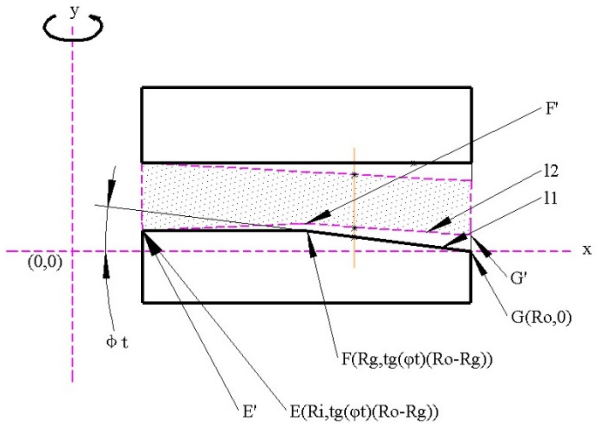

Fig. 5. Hydrostatic model of end face

As shown in Fig. 4 and Fig. 5, Establish a Cartesian coordinate, seal swirl around y axis, and the taper face outer point on the x axis. After the seal deflected (dash line), the points E, F, G will be translated to point E', F', G'. The function of straight line L1 and L2 can be established in two points form:

L1:

$$y = -tan(\varphi_t) \cdot x + R_O \cdot tan(\varphi_t) \quad (1)$$

L2:

$$\frac{y-y_{G'}}{y_{F'}-y_{G'}} = \frac{x-x_{G'}}{x_{F'}-x_{G'}} \quad (2)$$

For L2, $y_{G'}$, $x_{G'}$, $y_{F'}$, $x_{F'}$ in (2) is the horizon position and vertical position of point G and F after seal deflection which can be carried out by rotating coordinates formula simply. Once this four positions has been got. Take them into (2), and then the linear function of L2 is:

$$y = -\frac{1}{sin(\varphi_r)\,tan(\varphi_t)+cos(\varphi_r)}\Big(\big((R_i - R_O)\,cos(\varphi_r)\big) + tan(\varphi_t)\Big)$$
$$(R_g - R_o)\,sin(\varphi_r) + x - R_i)(cos(\varphi_r)\,tan(\varphi_t) - sin(\varphi_t))) + (cos(\varphi_t) - 1)(R_g - R_o)\,tan(\varphi_t) + (R_o - R_i)\,sin(\varphi_r) \quad (3)$$

Assume the variable $R \subseteq (R_g, R_o)$ and position of points B and D are known as $(X_{B'}, Y_B)$, $(X_{D'}, Y_D)$. Then L_{BD} the distance between B and D is:

$$L_{BD} = \frac{1}{sin(\varphi_r)\,tan(\varphi_t)+cos(\varphi_r)}(-sin(\varphi_r)(R - R_g)\,tan(\varphi_t)^2 - (cos(\varphi_r)^2 + sin(\varphi_r)^2 - cos(\varphi_r))(R_g - R_i)\,tan(\varphi_t) - sin(\varphi_r)(R - R_i)) \quad (4)$$

Film thickness control function h(R):

The film thickness control function on whole end face can be divided into two parts. One is parallel region $R \subseteq (R_i, R_g)$ and another is taper region $R \subseteq (R_g, R_o)$. "h_1" is the film thickness before seal deflecting and "h'" is that after seal deflecting. Then:

The parallel region film thickness h_a is:

$$ha = h_1 - (R - R_i) \cdot \tan(\varphi_s) - (R - R_i) \cdot \tan(\varphi_r) \quad (5)$$

The taper region film thickness h_b is:

$$ha = h_1 + \tan(\varphi_t) \cdot (R - R_g) - (R - R_i) \cdot \tan(\varphi_s) - L_{BD} \quad (6)$$

Take (4) into (6), the taper region film thickness h_b is:

$$h_b = h_1 + tan(\varphi_t)(R - R_g) - (R - R_i)\,tan(\varphi_s) + tan(\varphi_t)R - tan(\varphi_t)R_o - \frac{1}{sin(\varphi_r)\,tan(\varphi_t)+cos(\varphi_r)}(((R_i - R_o)\,cos(\varphi_r) + tan(\varphi_r)(R_g - R_o)\,sin(\varphi_r) + R - R_i)(cos(\varphi_r)\,tan(\varphi_t) - sin(\varphi_r))) + (cos(\varphi_r) - 1)(R_g - R_o)\,tan(\varphi_t) + (R_o - R_i)\,sin(\varphi_r) \quad (7)$$

The film thickness profile after seal deflected can be plotted as Fig. 6 once φ_r and φ_s are obtained.

Assume the media of RCP seal is uncompressible. The scale of film thickness is much smaller than that in faceplate direction. Therefore, the 2D Reynolds equation in pole coordinate is suitable[10-11]:

$$\frac{1}{R}\frac{\partial}{\partial\theta}\left(\frac{h^3}{12\mu}\frac{\partial p}{\partial\theta}\right) + \frac{\partial}{\partial R}\left(\frac{rh^3}{12\mu}\frac{\partial p}{\partial R}\right) = \frac{R\omega}{2}\frac{\partial h}{\partial\theta} \quad (8)$$

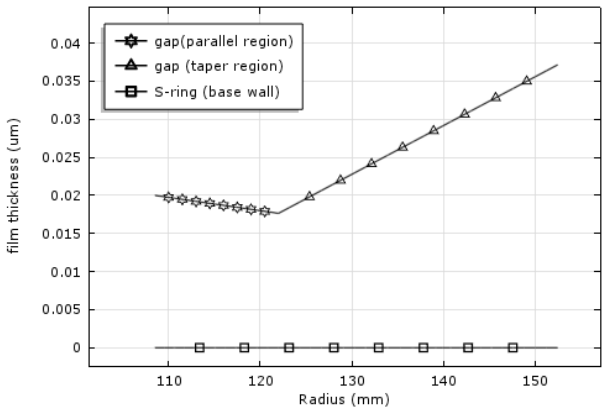

Fig. 6. The film thickness profile of the end face (assume $\varphi_r = 0.367', \varphi_s = 0.046'$)

For RCP hydrostatic seal, the pressure and thickness gradient along pole angle θ is equal to 0. It means $\frac{\partial p}{\partial \theta} = \frac{\partial h}{\partial \theta} = 0$, so that (8) can be simplified into:

$$\frac{\partial}{\partial R}\left(\frac{Rh^3}{12\mu}\frac{\partial p}{\partial R}\right) = 0 \quad (9)$$

Take (5) or (7) into (9), the end face pressure distribution function P(R) with two subsections can be obtained. It is difficult to carry out an explicit solution about the P(R). A program written in Matlab based on FE method is used to solve numerical solutions. The detail procedure of FE method can be found in reference[10]. A comparison between MTEHM and common hydrostatic model is taken out as instance:

The pressure distribution curves of these two models can be plotted as Fig. 7. An obvious difference can be found especially in parallel region ($R \subset (108,125)$ mm). The result of common hydrostatic model is approximate to linear but the MTEHM is a concave line. That means the area below the MTEHM curve is smaller. The end face open force is equal to this area. The film thickness and leakage under balance status is smaller than that of common hydrostatic model also. A further plot about how the taper changing influence end face pressure distribution is shown as Fig. 8

Table 1. Boundary conditions of MTEHM and common hydrostatic model

parameter	MTEHM	Common hydrostatic model	physics
h1	5[um]	5[um]	Film thickness(assumed)
RPM	1500	1500	Rotating speed (RPM)
φ_r	0.367	0	Rotating component deflection angle(minutes)
φ_s	0.0456	0	stationary component deflection angle(minutes)
φ_t	3	3	Initial taper (minutes)
T	55+273	55+273	injection temperature (K)
Rg	122[mm]	122[mm]	End face taper transition radius (mm)
Ri	108.5[mm]	108.5[mm]	Inner radius of end face(mm)
Ro	152.5[mm]	152.5[mm]	Outer radius of end face (mm)
Rb	121.4[mm]	121.4[mm]	Balance Radius (mm)
Roring	119.5[mm]	119.5[mm]	O-ring radius back of rings (mm)
P2	15.8[MPa]	15.8[MPa]	Media pressure (MPa)
P1	0.21[MPa]	0.21[MPa]	Leakage pressure (MPa)

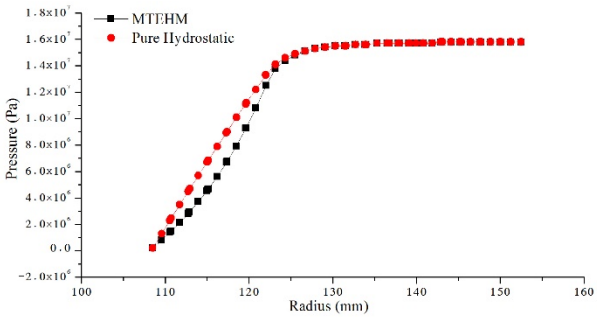

Fig. 7. The P(R) (MTEHM vs. common model)

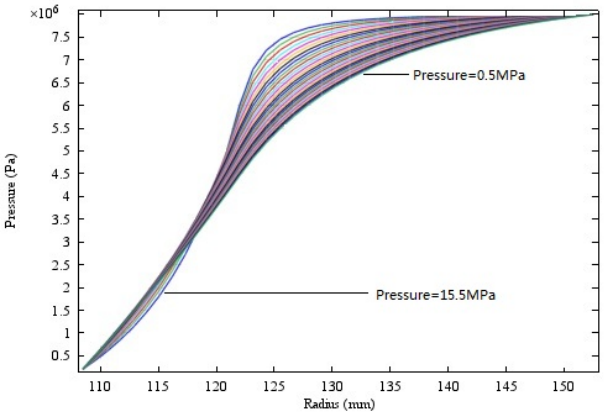

Fig. 8. P(R) with taper changing

In the instance above, the end face deflecting angle φ_r, φ_s are assumed to be known at the beginning. For closing the coupling circle, an Elastic-solid model with thermal condition and multi-body contacting is required to obtain the deflecting angle.

4. Thermal Elastic multi body contacting model

In this section, the interaction of the mechanical parts and temperature gradient are taken into solid model. According to experimental results, the differential temperature along radial direction of the end face is $4^\circ C \sim 8^\circ C$. It has a small variation when injection temperature or leakage changed. A FEA method with multi-body contacting and thermal condition is applied.

A 2D axial symmetry model which includes hydrostatic clamp rings, seal rings, ring seats and virtual shaft is assembled. All contact pairs have a different size of mesh and are set to be frictional as the A~G shown in Fig. 9. The friction coefficient is 0.37. Contact source has a fine size and contact target has a chaos size to prevent nodes from penetrating. The contact force is defined by:

$$F_{normal} = k_{normal} x_{penestration} \quad (10)$$

Where the k_{normal} is contact stiffness and $x_{penetration}$ is penetrating amount.

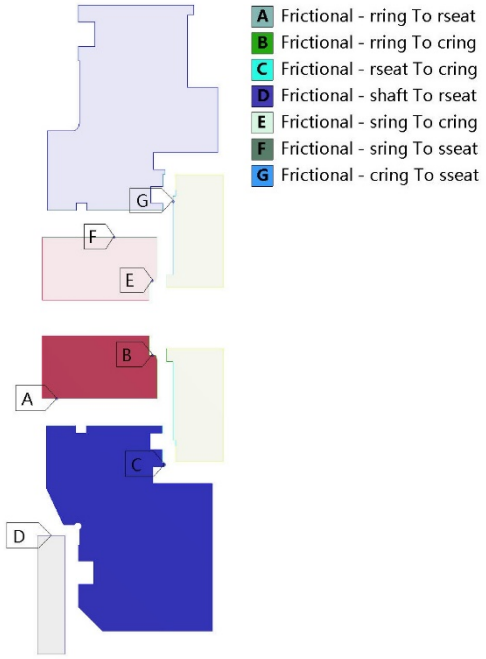

Fig. 9. multi-body contacting model of No.1 seal

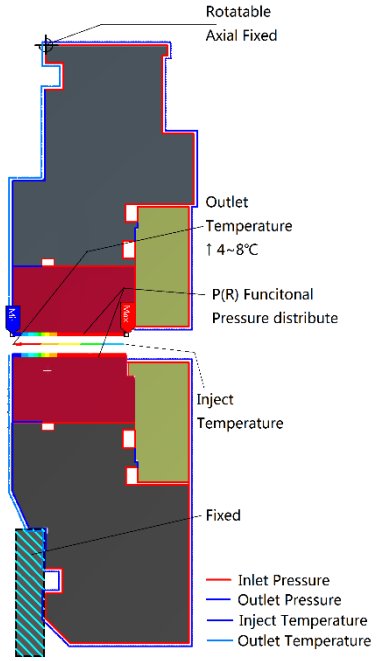

Fig. 10. Boundary conditions and constraint

4.1 Boundary Conditions, Constraints, Materials Property

Table 2. Loads, materials, work conditions

		Young's modular (GPa)	Poisson's ratio	Thermal conductivity (W/m*°C)
Rings	Si3N4	320	0.272	28.4
Clamp rings, ring seats	stainless steel	217	0.27	30
media	water	viscosity 5.1E-4Pa*s	Specific heat 4200J/kg*°C	0.645
Inlet pressure	15.8MPa		Inlet temperature	55℃
Outlet pressure	0.21MPa		Outlet temperature	60℃

The boundary condition applied in solid model is shown as Fig. 10. An interface program written in C language is used to transit the pressure value from fluid zone to solid zone automatically. Therefore, the coupling between fluid and solid zones is archived.

The calculation of temperature gradient of end face can be found in reference[12]. It is the same with reference [12], the solid thermal conductivity, and solid-fluid conjugate heat transfer is considered. Injection temperature, leakage, thermal conductivity, heat transfer coefficient will influence the end face temperature gradient.

Four probes located on end face of seal rings inner corner and outer corner are set to get the axial displacement. They are:

Rin —inner corner displacement of rotating ring, mm
Rout —outer corner displacement of rotating ring, mm
Sin —inner corner displacement of stationary ring, mm
Sout —outer corner displacement of stationary ring, mm

At last, the seal deflection angle φ_r, φ_s can be obtained by solving a triangle function simply.

4.2 Coupling processing

The solving program is beginning from fluid zone.

Step1: assume that the $\varphi_s = \varphi_r = 0$, and a sets of film thickness $|h| \supset h_{eq}$ are taken as input. h_{eq} is the film thickness when seal works in balance status。Use $F_{open} = F_{close}$ to evaluate whether the seal archives balance status or not. Then the end face pressure distribution P(R) can be obtained as output.

$$F_{open} = \int_0^{2\pi} P(R)\, d\theta \tag{11}$$

$$F_{close} = G + Po \cdot \pi \cdot (R_o^2 - R_b^2) - Pi \cdot \pi \cdot (R_b^2 - R_i^2) \tag{12}$$

Step2: the value of P(R) can be translated by interface program and be transferred to end face nodes in solid model. Other input containsT_o,T_i,$T(R)$,T_o, T_o is injection temperature, T_i is leakage temperature, and $T(R)$ is temperature gradient on the end face. The linear level of $T(R)$ influence seal deformation less. So the $T(R)$ is treated as linear in this study. The φ_s, φ_r can be obtained in this step as output.

Step3: Take the φ_s, φ_r back into Step1 to calculate the end face pressure distribution $P(R)_n$ again, n=1…n which means the iterative steps。

Step4: repeat Step1~Step3, and output $P(R)_n$ each time. It can be found that the open force by integrating the $P(R)_n$ will not decrease obviously after several repeats. Therefore, the coupling convergence criterion shall be:

$$\frac{\int_0^{2\pi} P(R)_n d\theta - \int_0^{2\pi} P(R)_{n-1} d\theta}{\int_0^{2\pi} P(R)_{n-1} d\theta} \leq 0.01 \quad (13)$$

Step5: the final solutions can be obtained by iterating n times and which include film thickness h_{eq_n}, leakage Q_n and end face open force F_{open_n}.

$$F_{open_n} = \int_0^{2\pi} P(R)_n \, d\theta \quad (14)$$

5. Discussion of Engineering Application

In order to confirm the engineering applicability of MTEHM, a test rig as shown in Fig. 11 has been established in Sichuan Sunny Seal Company. The Fig. 12 is the No.1 seal and its stationary ring after 4000 hours life circle experiment.

Fig. 11. Test rig for RCP hydrostatic seal

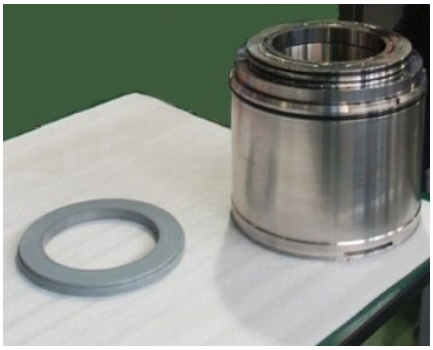

Fig. 12. No.1 seal disassembled

5.1 The Influence of Temperature

The temperature influences the viscosity and density of seal media mainly. The leakage increase as the temperature increase[12-15]. Except for that, the temperature influence end faces taper also, but much smaller than pressure. A comparison between pure pressure effect (Fig. 13) and pure thermal effect (Fig. 14) is shown as below Table 3 and Table 4:

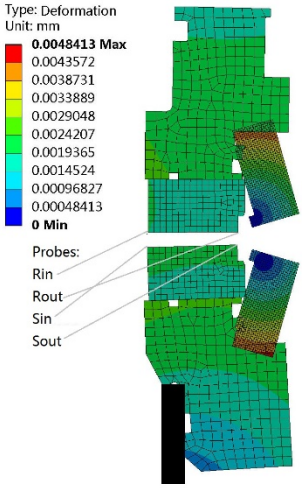

Fig. 13 Pressure effect (15.5MPa)

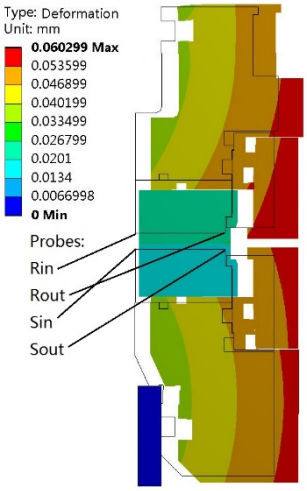

Fig. 14 Thermal effect (with 5℃ differential temperature)

Table 3. Seal deflection of single pressure effect (15.5MPa)

Probe		Axial displacement (mm)	End face width (mm)	Deflecting angle (minutes)	Total angle (minutes)
R-ring	Rin	1.34E-03	4.63E-03	0.3678	0.4135
	Rout	5.97E-03			
S-ring	Sin	-1.32E-03	5.75E-04	0.0456	
	Sout	-7.46E-04			

Table 4. Seal deflection of single thermal effect (with 5℃ differential temperature)

Probe		Axial displacement (mm)	End face width (mm)	Deflecting angle (minutes)	Total angle (minutes)
R-ring	Rin	1.5971e-2	2.80E-05	0.0022	0.0002
	Rout	1.5943e-2			
S-ring	Sin	-3.0729e-2	2.50E-05	0.0019	
	Sout	-3.0704e-2			

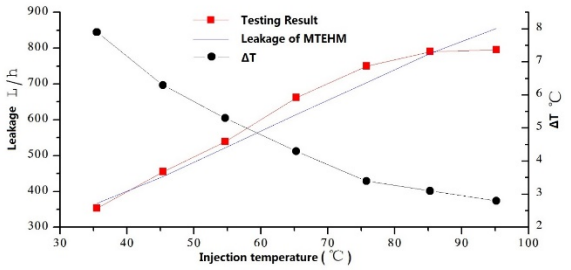

Fig. 15. Injection temperature VS. Leakage and ΔT (15.5MPa)

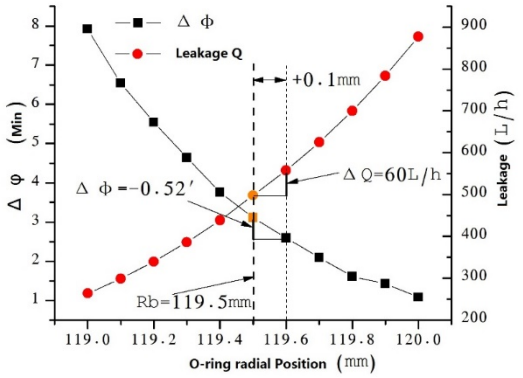

Fig. 16. The influence of radius O-ring on back of seal rings (15.5MPa, 55°C, up)

It can be observed from column "axial displacement" in Table 3 and Table 4 that the taper is divergent form R_o to R_i when seal subject to pressure only. On contrary the taper is convergent when seal subject to temperature only. And the "Total angle" column shows that the influence of pressure is more important than that of temperature.

Injection temperature influence the end face differential temperature and leakage. The higher injection temperature, the larger leakage is. The simulation and experiment results are shown in Fig. 15.

5.1 O-Ring Positions

There are two sets of O-rings influence leakage mainly. One is on back of the seal rings and another is a pair of O-rings on the hydrostatic clamp rings.

It is need to clarify that the O-rings' material is FKM[14]. When it is compressed by seal media with different pressure, the pressure boundary points will changing. In this study, the error caused by the boundary points offset has been ignored because of it is too tiny to influence the final results.

For the O-ring back of seal rings. Once the distributed pressure be treated as concentrated force, the origin and value of this force will be influenced by the radius of O-ring. And then the end face taper changed. Larger the radius of O-ring is, the pressure effective area is smaller, the end face taper variation $\Delta\varphi$ is smaller, the taper after deflecting φ' is larger, and the leakage is larger. With smaller radius, the changes are on contrary. As shown in Fig. 16:

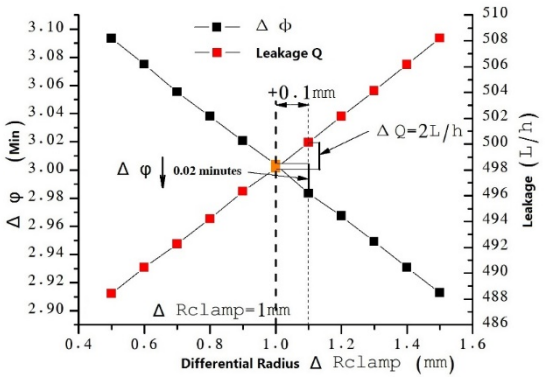

Fig. 17. Influence of differential radius of O-ring on clamp rings (15.5MPa, 55°C,below)

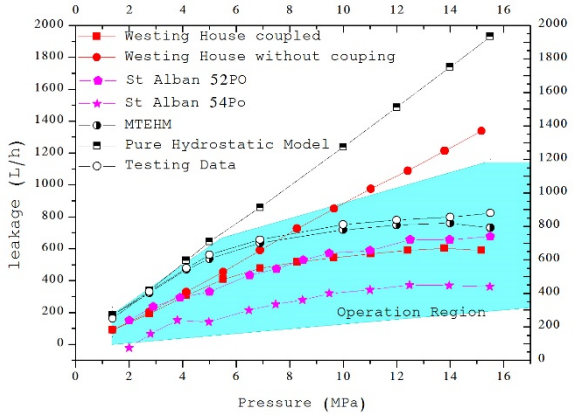

Fig. 18. Comparison of MTEHM, Westinghouse, St Alban and testing data

There are two O-rings with different radius of the hydrostatic clamp rings. The difference of radius of this two O-rings ΔR_{clamp} influence the axial load of clamp rings. The ΔR_{clamp} increased, the axial load increased. The end face taper deflecting angle $\Delta\varphi$ decreased as well. The end face net taper after deflecting φ' increased.

$$\varphi_t' = \varphi_t - \Delta\varphi \tag{14}$$

The leakage increased at last, shown as Fig. 17:

5.2 End Face Differential Pressure

It can be found from Fig. 18 that the leakage (with 55°C and 15.5MPa injection) obtained by MTEHM is close to which obtained by common hydrostatic model when inject pressure is blow 5MPa. But the leakage curve becomes more flat as the pressure increasing. This is because of the end face net taper decreasing. As shown in Fig. 18, this trend is same to Westinghouse's[3] and the real operation data from Saint Alban 52PO, 54PO[16]. There is a 200L/h leakage difference between MTEHM and Westinghouse's result because of different research targets' geometric dimensions. It can be adjusted by changing initial end face taper. The initial taper increased the leakage curve rise up entirely and it is the key parameter that influences the RCP No.1 seal's performance. And the optimize design points can be obtained by this MTEHM now.

6. Conclusions

A MTEHM has been presented in this study to simulate the RCP seal end face pressure-leakage relationship. The results display an obvious difference with pure hydrostatic model. Especially in the inner radius region of the end face. The pressure-leakage trend curve of MTEHM is concave. Different with that, the trend curve is convex of common pure hydrostatic model as shown in Fig. 7. The open force of MTEHM is 4.7% smaller than pure hydrostatic model(15.5MPa, 55℃).

According to the MTEHM results: the changing of end face net taper caused by pressure and changing of viscosity of media caused by injection temperature are key factors that influent RCP seal leakage directly. The changing cause by pressure is more important than by injection temperature as shown in Table 3 and Table 4. The viscosity of media decreased as the temperature increased and this lead to leakage increase directly as shown in Fig. 15. and it can be conclude that 43L/h leakage increasing when injection temperature increase 5℃ The secondary seal on two different locations influence the interior forces of the seal assembles. Compare the Fig. 16 with Fig. 17 and it can be conclude that the position variation of O-ring behind seal rings is more important than that of clamp ring's O-ring. Compare the Fig. 16 with Fig. 17 and it can be conclude that the radius of O-ring behind seal rings increase each 0.1mm, the leakage increase 60L/h. and the differential radius of clamp ring O-rings increase each 0.1mm, the leakage increase 2L/h. this conclusions above are obtained on conditions of 15.5MPa and 55℃ injection temperature.

The MTEHM can couple the influence of thermal effective, multi-body contacting effective, hydrostatic effective and rigid-flexible body deformation effective very well. The MTEHM results are approximate to simulation data from Westinghouse and real operation data from Saint Alban nuclear plant 52PO, 54PO as shown in Fig. 18. Except for that, It can be found in Fig. 18, the testing result about pressure-leakage curve match the MTEHM simulating result very well. That means this model can be used to predict the leakage behavior of RCP No.1 seal in engineering applications. And it can be used to optimize the design too.

References

1. C J Ruger and J C Higgins. Reactor Coolant Pump Seal Issues and Their Applicability to New Reactor Designs[R]//NUREG/49115, Brookhaven National Laboratory, Upton, NY, 1993.
2. Robert J, Lutz Jr, J Gene Zottola, etc. Westinghouse Owners Group Reactor Coolant Pump Seal Performance for Appendix R Assessments[R]. Prepared for Westinghouse owners Group, Developed under WOG Program, PA-RMSC-0181, Jan, 2005: 11-14.
3. T boardman, N jeanmougin, et al. Leak Rate Analysis of The Westinghouse Reactor Coolant Pump[R]// Research Report Prepared for U.S Nuclear Regulatory Commission, Energy Technology Engineering Center, 1985.
4. Erwan Galenne, Isabelle Pierre-Danos. Thermo-Elastic-Hydro -Dynamic Modeling of Hydrostatic Seals in Reactor Coolant Pumps [J]. Tribology Transactions, 2007, 50:466-476.
5. Brunetière N, Tournerie B and Frêne J. TEHD Lubrication of Mechanical Face Seals in Stable Tracking Mode [J]//Part1: Numerical Model and Experiments, ASME Journal of Tribology, 2003, 125(5): 608-616.
6. Wang Heshun, Zhu weibing, Huang Zepei, Zhang Chening. Main Pump Seal's Characteristics Affected by Cone Angle and Clearance [J]//TELKOMNIKA Indonesian Journal of Electrical Engineering, October, 2014, 12(10): 7233-7241.
7. Yasuhiro Sasaki, Kazuyuki Obata, Osamu Hisai, Toshihiko Matsuo, Naotaka Komatsu, Hidekazu Uehara. Improved Shaft Seal for 93A Type Reactor Coolant Pump [J]//Mitsubishi Heavy Industries, Technical Review, Feb, 2005, 42(1).
8. Liao C J, Huang W F, Suo S F, et al. fluid-solid strong-interaction model of mechanical seals in reactor coolant pumps [J]. Science china-technology sciences, 2011, 54(9): 2339-2448.
9. Huang Weifeng, Liao Chuanjun, Liu Xiangfeng, Suo Shuangfu, Liu Ying, and Wang Yuming. Thermal Fluid-Solid Interaction Model and Experimental Validation for Hydrostatic Mechanical Face Seals [J]. Chinese Journal of Mechanical Engineering, 2014, 27(5): 949-957.
10. Lebeck. Principles and Design of Mechanical Face Seals [M]. 1991: 153-155.
11. Xinmin Z, X Yanqiu, Z Qing, F Xin. Analysis for Rotordynamic Coefficients of Partially Tapered Short Annular Seals [J]. Lubrication Engineering, 2004, 163(3): 71-75.
12. Etsion I, Pascovici M D. A thermodynamic analysis of a misaligned mechanical face seal [J]. Tribology Transactions, 1993, 36(3): 589-596.
13. Zhenmin H, W Qinhu, C Zhipeng, H Ye. Theory Research and Application of Using Temperature Control Method to Avoid the Nuclear Main Pump High Stops Due on the 1st Shaft Seal High Leakage [J]. Pump Technology. 2008, (6): 7-13.
14. Dongbo M, C Jining, Z Qiuxiang, L Shuangxi. Study on the Seal Property of the Second Seals of Reactor Coolant Pump in Nuclear Station from Contacting to Non-contacting Mechanical Seal [J]. Lubrication Engineering. 2009, 34(7): 33-37.
15. Doust T G, Parmar A. An Experimental and Theoretical Study of Pressure and Thermal Distortions in Mechanical Seals [J]//ASLE Trans, 1986, 29(2): 151-159.
16. Tournerie B, J Frêne. Influence of Fluid Flow Regime on Performances of Non-Contacting Liquid Face Seals [R]. 2002.